Simulation of an Energy Self-sufficient Electrodialysis Desalination Stack for Salt Removal Efficiency and Fresh Water Recovery

Ying Mei [a], Xianhui Li [a], Zhikan Yao [b], Weihua Qing [c], Anthony G. Fane [d], Chuyang Y. Tang [a,d,e *]

[a] Department of Civil Engineering, The University of Hong Kong, Pokfulam Road, Hong Kong S.A.R., P.R. China

[b] College of Chemical and Biological Engineering, Zhejiang University, Hangzhou 310027, China.

[c] John A. Reif, Jr. Department of Civil and Environmental Engineering, New Jersey Institute of Technology, Newark, New Jersey 07102, United States

[d] UNESCO Centre for Membrane Science and Technology, School of Chemical Engineering, University of New South Wales, Sydney, New South Wales 2052, Australia

[e] UNSW Water Research Centre, School of Civil and Environmental Engineering, University of New South Wales, Sydney, New South Wales 2052, Australia

*Corresponding author address: HW6-19B Haking Wong Building, Department of Civil Engineering, the University of Hong Kong, Pokfulam, Hong Kong; Tel: (+852) 28591976; email address: tangc@hku.hk

Abstract

Electrodialysis is a commonly used desalination method. In this study, we investigate its hybridization with its reverse process, where reverse electrodialysis (RED) harvests the salinity gradient power to provide the driving force for electrodialysis. In particular, the desalination performance (rejection and recovery) and their tradeoff relationship are simulated for the first time for an energy self-sufficient RED-ED desalination stack (REDD). The simulation results show that these two parameters can be simultaneously optimized by tailoring ion exchange membranes in the stack, i.e., using more selective membranes in the ED sub-cell (ED_{cell}) and less selective membranes in the RED sub-cell (RED_{cell}). Our analysis shows that a considerable driving force (e.g., a salinity ratio of high salinity stream to low salinity stream over 30 and a volumetric ratio over 0.5) is required to fully unleash the desalination performance of REDD, leading to a favorable shift of the rejection-recovery tradeoff line. In addition, multi-pass treatment is demonstrated to further enhance rejection at the expense of lower recovery. Similarly, a multi-stage configuration can be applied for higher recovery. This study reveals the operational constraints of a novel desalination REDD technique and provides insights into performance enhancement.

Keywords: Reverse electrodialysis (RED); Electrodialysis (ED), Hybrid process, Energy self-sufficient desalination, Rejection-recovery tradeoff

Graphical Abstract

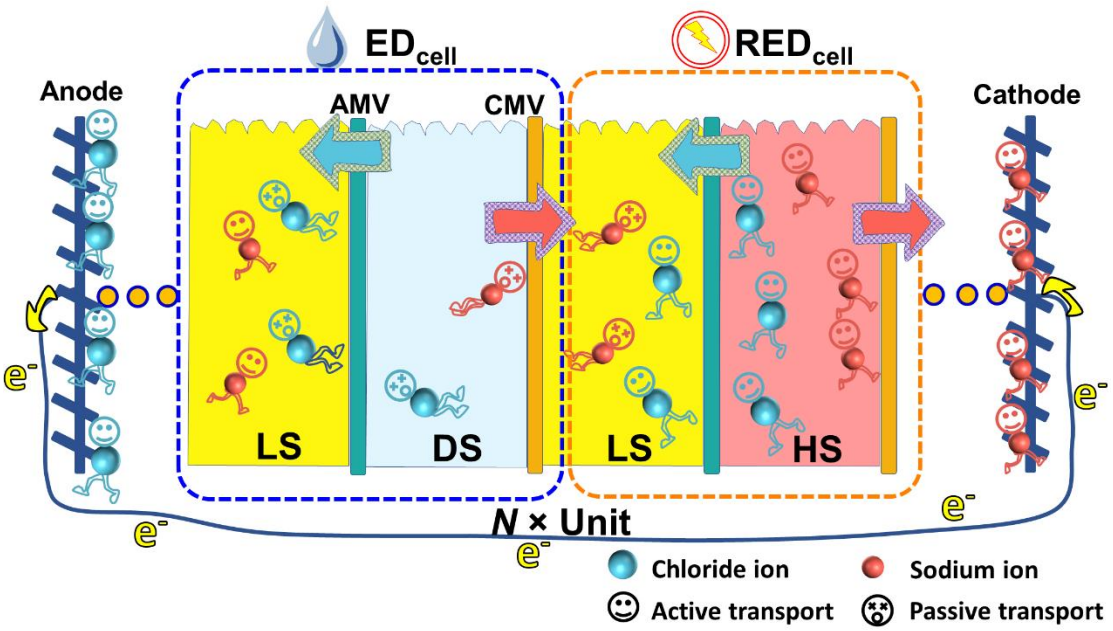

1. Introduction

Conventional desalination processes, such as reverse osmosis (RO), membrane distillation (MD) and electrodialysis (ED), are relatively energy intensive [1, 2]. Therefore, exploring reliable and more energy-efficient desalination methods is of great importance to alleviate worldwide water scarcity. Interestingly, brine, a high salinity (HS) byproduct of desalination that is often associated with adverse environmental impacts [2, 3], provides us a way to offset the energy required for desalination [4-7]. Controlled mixing of the brine with a low salinity stream (LS, e.g., treated wastewater) can generate a considerable amount of salinity gradient energy (SGE) [6, 8-10]. Among the various technologies for harvesting SGE, reverse electrodialysis (RED) has become a promising candidate. In RED, cations and anions transport through ion exchange membranes (IEMs) under their respective gradient, converting salinity gradient based chemical potential to electricity [8, 11-14]. In addition to the energy recovery, this controlled mixing in RED dilutes the brine, which also helps to reduce its adverse environmental impacts when discharged.

Sevaral researchers have investigated ways to integrate RED with desalination technologies [2, 5, 7, 9, 15-22]. For example, Li et al. [2] explored the conceptual design of RED-RO hybrid system, in which RED can be used either as pre-treatment (for reducing osmotic pressure of seawater) or post-treatment (for diluting the brine) to RO. In both arrangements, the specific energy consumption for desalination can be potentially reduced by more than half. A series of investigations have also been performed on hybrid RED-MD systems, in which the highly concentrated and warm brine provided by MD could enhance the RED energy generation [7, 21-23]. Recently, hybridization of RED with ED has also been reported [5, 9, 15, 24]. This configuration

shows unique benefits for allowing direct ultilization of the RED-generated electricity in the ED process. In comparison, hybridization of ED with pressure retarded osmosis (PRO), an alternative process for SGE harvest [11, 12, 25-27], requires the conversion of mechanical energy from PRO to electrical energy for driving ED. Therefore, the RED-ED hybrid system offers key advantages of higher energy conversion efficiency, together with simplified process configuration [5, 9, 15, 24] and potentially reduced fouling risks compared to the PRO-based schemes [28-31].

Previous RED-ED studies have explored its performance under various operating conditions, process configurations through simulation and experimental measurements [5, 9, 15, 24]. However, little is known about the performance in terms of fresh water recovery and equivalent salt rejection which are important parameters of interest for a typical desalination process. Moreover, in conventional desalination processes, increasing the fraction of water recovered typically deteriorates the quality of the produced water, and vice versa. Nevertheless, this important tradeoff relationship has not been explicitly discussed in the context of RED-ED hybrid desalination systems. This is a critical knowledge gap that has to be systematically addressed to evaluate process viability. The paramount importance of the tradeoff between salt removal and water recovery has prompted us to systematically investigate their relationship under various conditions, including the use of different membranes and process configurations.

In this study, we investigated an energy self-sufficient RED-ED desalination stack (REDD) where the salinity gradient power harvested by the RED process was used to drive the ED process. Its desalination performance was systematically investigated

through model simulation and experimental verification. Additional operating configurations (multi-pass vs. multi-stage) were also explored. Our study establishes the inherent tradeoff relationship between the recovery and the equivalent salt rejection for the RED-based hybrid desalination, which provides important insights into performance constraints of this novel desalination technology.

2. Process description and theoretical simulation

The novel REDD process contains repeating self-sufficient desalination units (Fig. 1). Each repeating unit is comprised of (1) an RED sub-cell (RED_{cell}) that generates electricity from the salinity gradient provided by a HS and a LS stream and (2) an ED sub-cell (ED_{cell}) that removes salts from a diluent stream (DS). This direct coupling of RED_{cell} with ED_{cell} enables energy self-sufficient desalination by using RED as the sole source of driving force for desalination in ED. Furthermore, this integrated RED-ED configuration requires only one pair of electrodes at the end of the REDD stack, which reduces the cost and electrical resistance associated with electrodes. The ionic spieces in the REDD stack (1) either transport from HS to LS under the salinity gradient in RED_{cell} or (2) are driven from DS to LS to maintain the electroneutrality in LS. As a result, salt is removed from DS, whereas the salinity gradient in RED_{cell} is reduced. During this process, an external current is also established (Fig. 1).

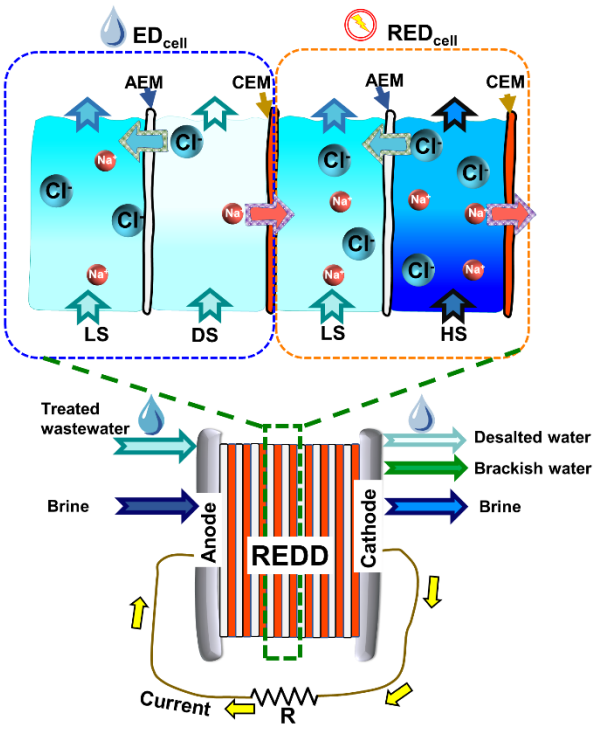

Fig. 1. Schematic diagram of an REDD stack and its repeating unit which comprises an ED_{cell} and an RED_{cell}. The input streams of HS (e.g., brine) and LS/DS (e.g., treated wastewater) are converted to diluted brine, brackish water and desalted water by the REDD stack. In the RED_{cell}, ions are driven through the ion exchange membranes by the salinity ratio of high salinity stream to low salinity stream (HS and LS). In the ED_{cell}, ions in diluent stream (DS) traverse against the concentration gradient from DS to LS using RED_{cell} as the energy source.

2.1. Simultation of the charge transfer in the REDD stack

The key to evaluating the desalination performance of an REDD stack is to quantifying the quality and the quantity of generated fresh water (i.e., DS). Our current analysis considers a batch desalination process. In a typical batch mode operation, both the solution concentrations and electrical current change over time and these quantities affect each other in accordance to Faraday's law [12]. Therefore, the instant salt concentration in each water compartment can be calculated as the sum of the initial salt concentration and the accumulative mass transfer (+ sign for transporting in and - sign

for transporting out of a given water compartment) which is converted from the corresponding coulombs of charge.

Consider the electrical loop in Fig. 1, the net electrical potential (E_{net}) can be formulated by the modified Nernst equation which accounts for the voltage provided by the RED_{cell} and that consumed by the ED_{cell} as follows [32-34]:

$$E_{net} = \underbrace{N\frac{RT\alpha_{RED}^{CEM}}{z^{+}F}\ln\frac{a_H}{a_L} + N\frac{RT\alpha_{RED}^{AEM}}{z^{-}F}\ln\frac{a_H}{a_L}}_{\text{(Voltage generation by RED)}} \underbrace{- N\frac{RT\alpha_{ED}^{CEM}}{z^{+}F}\ln\frac{a_L}{a_D} + N\frac{RT\alpha_{ED}^{AEM}}{z^{-}F}\ln\frac{a_L}{a_D}}_{\text{(Voltage drop by ED)}} \quad (1)$$

where N is the number of repeating units, R is the gas constant (8.314 J/mol·K), T is the absolute temperature (K), F is the Faraday constant (96,485 C/mol), α is the membrane permselectivity, z is the fixed charge of a certain ion (e.g., $z^+ = z^-=1$ for the model salt NaCl used in the current study), and a denotes the activity of the solution in each compartment where the subscript H stands for HS, L for LS, and D for DS. In this study, the solution activity was approximated by the concentration value without significantly affecting the simulation results. The subscripts *RED* and *ED* associated with α stand for the membranes used in the RED_{cell} and the ED_{cell}, respectively, while the superscript *CEM* and *AEM* refer to the cation exchange membrane and the anion exchange membrane, respectively. For simplicity and practical reasons, we further assume that $\alpha_{RED}^{CEM} = \alpha_{RED}^{AEM}$ and $\alpha_{ED}^{CEM} = \alpha_{ED}^{AEM}$.

In each repeating unit, it is assumed that the initial DS concentration equals the initial LS concentration, i.e., $c_{D0} = c_{L0}$, thereby the voltage of REDD (E_{net}) is generated by the salinity ratio in RED_{cell} (c_{H0} / c_{L0}) at the initial state. Then E_{net} decreases with time

as the voltage produced by RED_{cell} (c_H / c_L) needs to overcome the voltage barrier produced by the salinity ratio in ED_{cell} (c_L / c_D). Both of these ratios approach an equilibrium constant (*f*) which can be given by:

$$f = \frac{c_{Hf}}{c_{Lf}} = \frac{c_{Lf}}{c_{Df}} \tag{2}$$

where the subscript *f* refers to the final state.

Before achieving the final state, current density (*J*) changes with the voltage (E_{net}) and the total resistance in accordance to Ohm's law [35]:

$$J = \frac{E_{net}}{A \cdot \left(R_{stack} + R_{external} \right)} \tag{3}$$

where *A* stands for the active cross-sectional area of each membrane sheet, R_{stack} indicates the total internal resistance of the stack and can be approximated as follows [12, 34, 36]:

$$R_{stack} = \underbrace{\frac{N}{A}\left(\overline{R}_{RED}^{CEM} + \overline{R}_{RED}^{AEM} + \frac{\lambda_H}{\sigma_H c_H} + \frac{\lambda_L}{\sigma_L c_L} \right)}_{\text{(Resistance by RED)}} + \underbrace{\frac{N}{A}\left(\overline{R}_{ED}^{CEM} + \overline{R}_{ED}^{AEM} + \frac{\lambda_D}{\sigma_D c_D} + \frac{\lambda_L}{\sigma_L c_L} \right)}_{\text{(Resistance by ED)}} \tag{4}$$

where $\overline{R}$ describes the membrane area resistance with the subscript *RED* standing for the membranes in the RED_{cell} and *ED* for those in the ED_{cell}, and the superscript *CEM* refers to the cation exchange membrane and *AEM* to the anion exchange membrane, λ is the membrane thickness, σ denotes the molar conductivity of water streams with the subscripts *L*, *D*, and *H* referring to *LS*, *DS* and *HS*, respectively.

2.2. Simulation of mass transfer in the REDD stack

In an IEM, the current is preferentially carried by counter-ions (i.e., the ones with the

opposite charge to the membrane) rather than co-ions (i.e., the ones with the same charge as the membrane). To describe the portion of the overall current carried by the counter-ion, an intrinsic membrane parameter-transport number (T_{ct}^{m}) is applied [37]:

$$T_{ct}^{m} = \frac{z_{ct} j_{ct}}{z_{ct} j_{ct} + z_{co} j_{co}} \quad (5)$$

where j is the ionic flux, z is the ionic charge, the subscript ct and co indicate the counter-ions and co-ions, respectively. The transport number determines the permselectivity (α) of an IEM, i.e., $\alpha = \left(T_{ct}^{m} - T_{ct}^{s}\right) / T_{co}^{s}$, in which the superscript m and s stand for the transport number in the membrane matrix and bulk solutions, respectively [37]. The relationship between α and ionic flux of both co-ions and counter-ions through the membrane can be given as:

$$\alpha = \frac{j_{ct} - j_{co}}{j_{ct} + j_{co}} \quad (6)$$

Membranes in the hybrid system either operate in (1) the RED_{cell} where counter-ions transport along the salinity gradient from HS to LS in the same direction as co-ions; or in (2) the ED_{cell} where counter-ions transport against the salinity gradient from DS to LS in the opposite direction to co-ions [38]. Accordingly, the relationship between the charge (i.e., current) and ionic mass transport in the membranes also vary with the membranes' operation modes. Particularly, in the case of RED_{cell}, the current density (J) is given by the difference between the charge density carried by counter-ions (${j_{ct}}^{RED}$) and that by co-ions (${j_{co}}^{RED}$), i.e., $J = \left({j_{ct}}^{RED} - {j_{co}}^{RED}\right) \cdot F$. The mass transfer (${j_{mass}}^{H}$) away from HS can be determined by performing a mass balance and is given by the total flux of counter-ions and co-ions, i.e., ${j_{mass}}^{H} = {j_{ct}}^{RED} + {j_{co}}^{RED}$. Similarly, the current density (J) in the ED_{cell} is identical to the sum of the charge density carried by

counter-ions (j_{ct}^{ED}) and co-ions (j_{co}^{ED}), i.e., $J = \left(j_{ct}^{ED} + j_{co}^{ED} \right) \cdot F$, whereas the mass transfer (j_{mass}^{ED}) from DS is calculated as $j_{mass}^{D} = j_{ct}^{ED} - j_{co}^{ED}$, due to the opposite transport direction of co-ions and counter-ions. Combining these mass and charge balance expressions with Eq. (6) then yields the relationships between J and j_{mass} for each solution (i.e., HS, DS and LS). Specifically, the mass transfer in LS (j_{mass}^{L}) accounts for the ionic flux through the membranes both in RED_{cell} and ED_{cell} and is formulated as follows:

In HS:

$$\frac{J}{F} = \alpha_{RED} \cdot j_{mass}^{H} \tag{7}$$

In DS:

$$j_{mass}^{D} = \alpha_{ED} \cdot \frac{J}{F} \tag{8}$$

In LS:

$$\frac{J}{F} = \frac{1}{\left(\alpha_{ED} + \frac{1}{\alpha_{RED}} \right)} j_{mass}^{L} \tag{9}$$

Both the charge and mass transfer in an IEM change with time in the batch mode operation. Integrating Eqs. (7) ~ (9) with respect to the product of membrane area (A) and time (T) results in the relationships between the accumulative charge transfer and the total mass transfer for each solution as follows:

$$\int \frac{J}{F} A dt = \int \alpha_{RED} j_{mass}^{H} A dt \tag{10}$$

$$\int \frac{J}{F} A dt = \int \frac{1}{\alpha_{ED}} j_{mass}^{D} A dt \tag{11}$$

$$\int \frac{J}{F} A dt = \int \frac{1}{\left(\alpha_{ED} + \frac{1}{\alpha_{RED}}\right)} j_{mass}{}^{L} A dt \quad (12)$$

The accumulative mass transfer can be calculated by performing an ionic mass balance for each solution, i.e., $\int j_{mass}{}^{i} A dt = \frac{V_i \left| c_{i0} - c_{it} \right|}{N}$, where V is the water volume, the script i indicates the selected solution, the absolute value represents the difference between the concentration at the initial and final state. The total charge transport in the circuit can be given by Coulomb's law, i.e., $Q(t) = \int J A dt$. Substituting the above Eqs. into Eqs. (10) ~ (12) then yields the relationship between the salt concentration of each solution with charge transport:

$$c_{Ht} = c_{H0} - \frac{NQ(t)}{\alpha_{RED} V_H F} \quad (13)$$

$$c_{Dt} = c_{D0} - \frac{\alpha_{ED} NQ(t)}{V_D F} \quad (14)$$

$$c_{Lt} = c_{L0} + \frac{NQ(t)}{\alpha_{RED} V_L F} + \frac{\alpha_{ED} NQ(t)}{V_L F} \quad (15)$$

In the current study, it is assumed that the DS and the LS have identical initial concentrations at the beginning of the batch mode operation, i.e., the same low concentration solution is supplied for DS and LS. Consequently, a parameter $\bar{q}$ can be defined to quantify the salt removal efficiency of the REDD stack from the low salinity streams (i.e., DS and LS):

$$\bar{q} = \frac{(c_{D0} - c_{Dt}) V_D}{c_{D0} (V_L + V_D)} \quad (16)$$

where the volumetric ratio of the LS to the total volume of LS and DS, i.e., $V_D/(V_L+V_D)$, is defined as fresh water recovery (γ), and the ratio of decreased concentration to the initial concentration of DS, i.e., $(c_{D0}-c_{Dt})/c_{D0}$, is defined as equivalent salt rejection (φ):

$$\gamma = \frac{V_D}{V_L + V_D} \tag{17}$$

$$\varphi = \frac{c_{D0} - c_{Dt}}{c_{D0}} \tag{18}$$

In this study, all the simulation works were carried out in MATLAB software.

3. Model verification

3.1 Materials and experimental methods

3.1.1. Electrolyte and solutions

The feed streams applied in this study were prepared by dissolving specific amount of sodium chloride (NaCl, Uni-chem, Serbia) in Millipore water (Millipore Integral 10 Water Purification System). The end electrolyte rinse solution for the redox reaction was consisted of 0.05 M potassium ferricyanide (III), 0.05 M potassium ferrocyanide (II) (VWR, America) and 0.3 M sodium chloride.

3.1.2. Ion exchange membranes and module configuration

The cation exchange membranes (CEMs) and anion exchange membranes (AEMs) used in the current study were Selemion® CMV and AMV, respectively, obtained from Asahi Glass Engineering Co., Ltd. Japan. The detailed characteristics of the membranes are summarized in Table 1.

Table 1. Specific parameters of ion exchange membranes (IEMs) used in current study

Membrane	Type	Permselectivity [a]	Area Resistance ($\Omega \cdot cm^2$) [b]	Thickness (μm) [c]
CMV	CEM	> 0.9	3	120
AMV	AEM	> 0.9	2.8	120

[a] Membrane permselectivity is provided by the manufacturer.

[b] Membrane area resistance is measured by the manufacturer in 0.5 M NaCl solution.

[c] Membrane thickness in the swollen state is provided by the manufacturer.

The design of the REDD stack was adapted from a conventional RED stack used in our lab [6]. It was mainly composed of five repeating units sandwiched between two poly(methyl methacrylate) end plates. Each unit comprised four independent flow channels of which two were for HS and LS in the RED_{cell} and two for LS and DS in the ED_{cell}. All the water channels were confined by silicone gaskets and spacers (300-35/71, Sefar, Switzerland) with a thickness of 200 μm. The end plates were embedded with Ru/Ir oxide coated titanium electrodes (Sun Wing Technology Company, Hong Kong) and recirculated with electrolyte rinse solution which contained redox couple for converting the ionic current into electricity. The experimental setup was connected to an external electrical load with a constant resistance of 0.6 Ω (RS Components Ltd. Hong Kong), providing a closed loop for the continuous ionic mitigation in the system.

3.1.3. Process operations

Synthetic sodium chloride solutions with various concentrations were applied to investigate the REDD stack performance in a batch mode operation under different

scenarios with the following initial conditions:

(1) S-R-R, i.e., using seawater (0.6 M NaCl) as HS and river water or brackish water (0.02 M NaCl) as both LS and DS;

(2) B-R-R, i.e., using desalination brine (1.2 M NaCl) as HS and river water or brackish water (0.02 M NaCl) as both LS and DS;

(3) B-S-S, i.e., using desalination brine (1.2 M NaCl) as HS and seawater (0.6 M NaCl) as both LS and DS.

All feed streams were pumped into the stack at a constant flow rate of 14 mL/min per flow channel (corresponding to a linear flow rate of 1.2 cm/s), while the electrolyte was recirculated at 60 mL/min (corresponding to a linear flow rate of 1 cm/s). Prior to desalination experiments, the stack was operated in open circuit mode to reach a steady state, then it was short-circuited with the nominal external load of 0.6 Ω. The concentration and mass variation of each stream were monitored online by a conductivity meter (alpha conductivity 500, Eutech, Thermo Fisher Scientific Inc.) and an analytical balance (OHAUS Instruments Co., Ltd. China) throughout the experiments, respectively. A galvanostat (Zennium, ZAHNER-Elektrik GmbH & Co. KG, Germany) was applied to record the voltage drop over the external load which can be converted into the current of the stack by Ohm's law. All the experiments were conducted at ambient temperature (~ 25 °C).

3.2. Model verification

Fig. 2 shows the experimental concentration of each stream and the current as a

function of operating time for the three different cases. In all the cases, LS concentration increased with time. Whereas, both the HS and DS concentrations decreased over time before achieving an equilibrium state, where the current became neglegible. The changes in the solution concentrations were much faster at the beginning and then slowed down. It is attributed to the reduced driving force from the salinity gradient between HS and LS and the simultaneously increased electrical barrier from the salinity gradient between LS and DS. The simulation results based on Eqs. (13) ~ (15) agree well with these experimental observations. It is also noteworthy that a higher quality of desalted water (i.e., lower c_D) can be obtained in the presence of a high salinity difference in RED_{cell} (e.g., for the scenarios of S-R-R and B-R-R), which allows the use of shorter operation time and/or less membrane area (i.e., a smaller $A \cdot T$ product). The better desalination performance of these two cases can be explained by more efficient ionic transport as a result of the larger driving force, which can be well predicted by the simulation results.

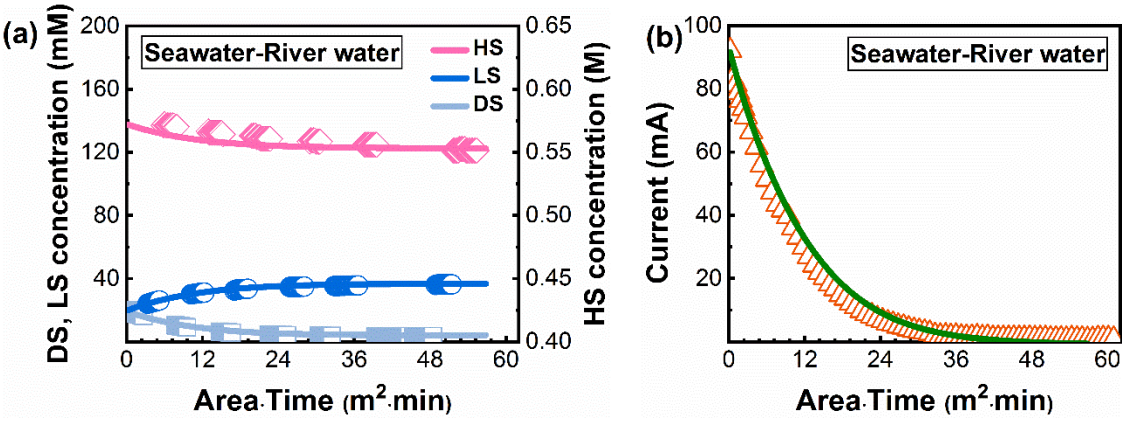

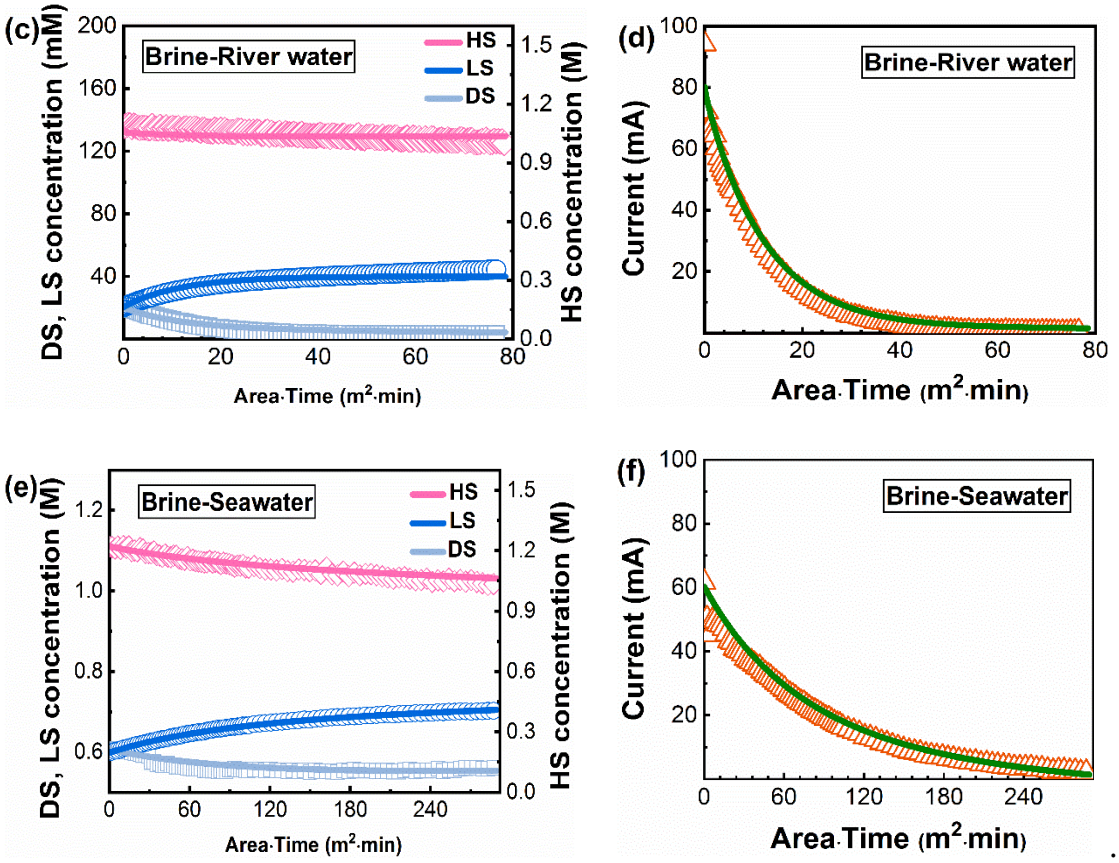

Fig. 2. Typical output curves of the REDD stack (N = 5, A = 0.0104 m^2, $R_{external}$ = 0.6 Ω) under three different operation conditions that the initial concentrations of HS and DS/LS (c_{D0}=c_{L0}) are set at: (a-b) 0.6 M and 0.02 M, respectively; (c-d) 1.2 M and 0.02 M, respectively; (e-f) 1.2 M and 0.6 M, respectively. Specifically, (a), (c) and (e) represent the concentration of each solution versus the product of operation time and total membrane area (i.e., Area·Time); (b), (d) and (f) show the discharge current versus Area·Time. The experimental results are shown as discrete symbols, while the simulation results are plotted as continuous curves. For the simulation, the recovery was fixed at 0.33.

4. Simulation results and discussion

In this section, the focus is on the role of membrane properties, operating conditions, and system configurations in determining the desalination performance of an REDD stack, based on the theoretical model described in *Section 2*. Specifically, the equivalent salt rejection ("rejection" for short in the following context) and the fresh water recovery ("recovery" for short in the following context) were simulated by Eqs.

(17) and (18), respectively. The final concentrations of DS were calculated by coupling the concentration equation (i.e., Eq. (14)) with the total charge transfer (i.e., $Q(t) = \int JAdt$) which can be given by the integration of Eq. (3) with time. According to the mathematical modelling, it is evident that the membrane properties determine both the electrical driving force (based on Eq. (1)) and the mass transport efficiency (based on Eqs. (7) ~ (9)), thereby affecting the overall desalination performance. The operational conditions also play a critical role. For example, the trans-membrane salinity in RED_{cell} ($\bar{c}_{H0}$) and the volume ratio of the HS over the sum of LS and DS ($\overline{V}_H$) determine the initial electrical driving force (Eq. (1)) and the rate of change of feed streams salinities. In the current study, the effects of these parameters were systematically investigated by changing one or more selected parameter(s) at a time while keeping the others constant. Unless otherwise specified, the following reference values were applied:

- Initial LS and DS concentrations: $c_{L0} = c_{D0}$ = 0.02 M (representing brackish water)
- Initial salinity ratio of c_{H0} to c_{D0}: $\bar{c}_{H0}$ = 30, i.e., c_{H0} = 0.6 M (representing seawater)
- Ratio of the DS volume to the total membrane area: V_A^D = 4.8 L/cm^2
- Volumetric ratio of V_H to the sum of V_D and V_L: $\overline{V}_H$ = 1

All other simulation conditions are specified in the relevant figure captions.

4.1 The effects of membrane properties on desalination performance

This section evaluates the role of membrane properties (i.e., membrane permselectivity

and resistance) in determining the desalination performance of an REDD stack. As discussed in *Section 2.2*, membrane permselectivity determines the electrical driving force (Eq. (1)) and the ionic mass transport which is converted from the electrical current (Eqs. (7) ~ (9)). In the study, two separate sets of membranes were applied in the RED_{cell} (α_{RED}) and the ED_{cell} (α_{ED}), respectively. Correspondingly, the investigation of membrane permselectivity was conducted for two scenarios: (1) varying α_{RED} with assuming that α_{ED} equals to α_{RED}; (2) varying α_{ED} with fixing α_{RED} at its reference value of 0.9.

Fig. 3 shows the rejection and the recovery of REDD as a function of the IEMs permselectivity (i.e., $\alpha_{RED} = \alpha_{ED}$). It is evident that both the rejection and the recovery are enhanced at increased α_{RED}. The results agree well with the theoretical analysis that IEMs with better permselectivity are apparently preferred. This is explained by the enhanced initial electrical driving force (i.e., higher E_{net} in Eq. (1)), the slowed decrease of the salinity gradient in RED_{cell} (i.e., smaller j_{mass}^{H} in Eq. (7)), and more efficient ionic transport (i.e., larger j_{mass}^{D} in Eq. (8)). The discrete points in the figure correspond to commercial and tailor-made IEMs reported in the literature as shown in Table A1 of Appendix A. The readers are also referred to Guler et al. [39] for a more comprehensive discussion of the properties of IEMs. In Figure 3, the membranes generally have relatively high permselectivity (> 0.8) [33, 34, 39-41]. These membranes yield a rejection of around 0.9 and a recovery of approximately 0.5. The slight shift of the discrete points from solid/dashed line in Fig. 3 can be attributed to the difference between membrane resistance of the commercial/tailor-made membranes (Appendix A.1, Table A.1) and the assumed membranes with the same

permselectivities.

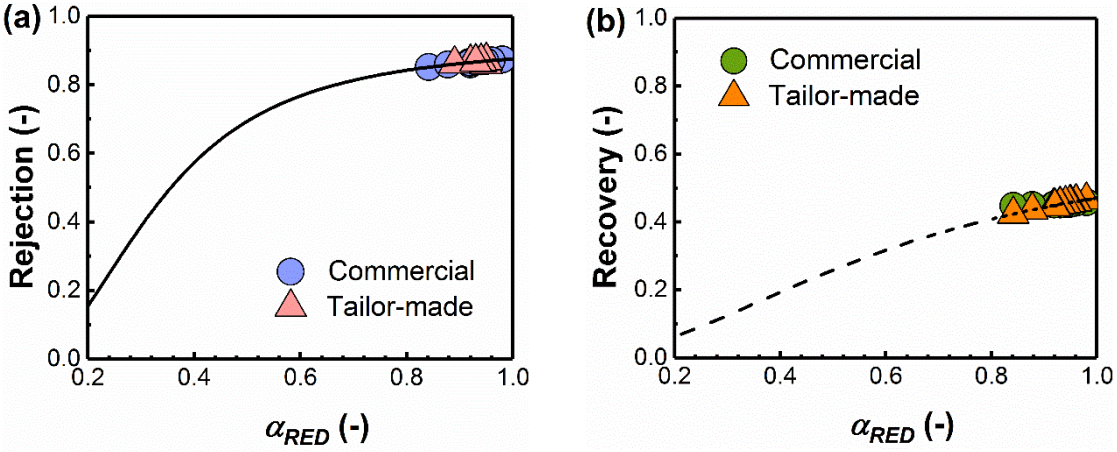

Fig. 3. Performance evaluation (based on modelling work) of an REDD stack for both commercial and tailor-made membranes (scatters) and for the membranes with an assumed permselectivity ($\alpha_{RED} = \alpha_{ED}$) ranging from 0.2 to 1.0 (solid line in (a) and dashed line in (b)): (a) equivalent salt rejection versus α_{RED} at a constant recovery of 0.33 (solid line); (b) fresh water recovery versus α_{RED} at a constant equivalent rejection of 0.8 (dashed line). The REDD stack (N = 5, A = 104 cm^2, $\lambda_H = \lambda_D$ = 0.2 mm) is short-circuited with an external load of 0.6 Ω. The membrane resistance values of the discrete points are adopted from the literature (Appendix A.1, Table A.1), while the resistance values of solid/dashed line are set as: $\bar{R}_{CEM}^{H} = \bar{R}_{AEM}^{H}$ = 3 Ω·cm^2, $\bar{R}_{CEM}^{D} = \bar{R}_{AEM}^{D}$ = 26 Ω·cm^2. The initial concentrations of HS is 0.6 M and DS/LS is 0.02 M; the molar conductivity of HS is 0.009 m^2/Ω·mol and DS/LS is 0.012 m^2/Ω·mol, while the recovery and $\bar{V}_H$ are fixed at 1/3 and 1, respectively.

We performed additional simulations to investigate the dependency of the desalination performance on α_{ED} while maintaining a constant α_{RED} at 0.9. At a fixed recovery of 0.33 and 0.5 (Fig. 4(a)), increasing α_{ED} decreases the rejection monotonically. However, at higher recoveries of 0.67, rejection increases first then decreases, resulting in an optimal rejection at relatively low α_{ED} values (< 0.4) at each given recovery. Similarly, at a fixed rejection, the recovery is optimized at a very low α_{ED} value (< 0.3) (Fig. 4(b)).

These results are counter-intuitive: the use of leaky IEM with permselectivity far lower than commercially available ones in the desalination cells enhances the overall desalination performance. These surprising results arise from the fact that a high permeability to co-ions leads to the slowed increase of LS concentration (i.e., smaller j_{mass}^{L} in Eq. (9)), thereby maintaining a relatively low electrical barrier in ED_{cell} for a longer time at the expense of minor losses on the salt removal rate ((i.e., smaller j_{mass}^{D} in Eq. (8)). As a result, enhanced accumulative mass transfer and ultimately greater rejection can be achieved. In comparison, using tighter IEMs (i.e., the one with better permselectivity) in ED_{cell} primarily achieves a faster salt removal, but simultaneously suffers a sharp increase in LS salinity and thus reduces electrical driving force within a short time. From this perspective, IEMs with low to moderate permselectivity can be a better alternative to the existing commercial IEMs for ED_{cell} to optimize the overall desalination performance. This is of practical relevance due to the fact that leaky IEMs are generally easy to fabricate and are of high ionic conductivity which will further increase the energy efficiency of REDD stack.

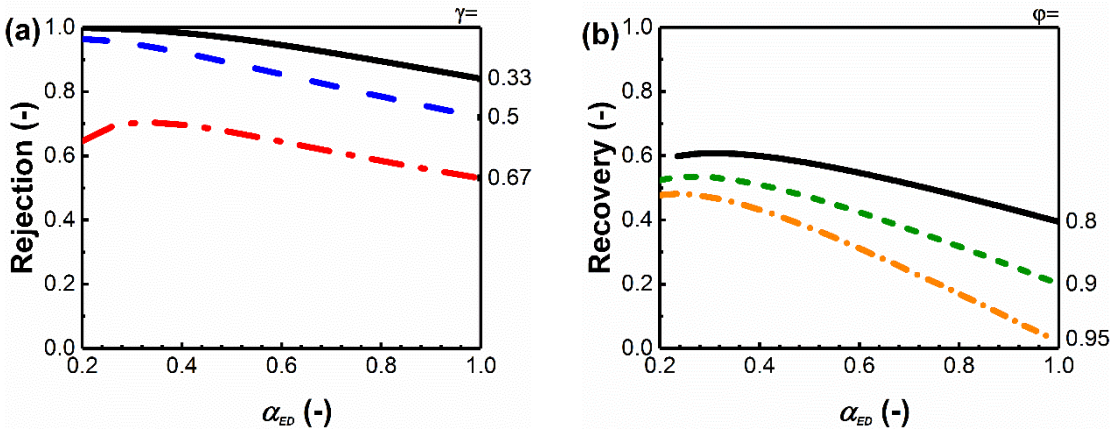

Fig. 4. Performance evaluation (based on modelling work) of an REDD stack for the membranes in the ED_{cell} with a permselectivity (α_{ED}) ranging from 0.2 to 1.0, while fixing the membrane permselecitivity (α_{RED}) in the

RED_{cell} at 0.9: (a) equivalent salt rejection versus α_{ED} at a series of recoveries; (b) fresh water recovery versus α_{ED} at a series of equivalent rejection. The REDD stack (N = 5, A = 104 cm^2, $\lambda_H = \lambda_D$ = 0.2 mm, $\bar{R}_{CEM}^{H} = \bar{R}_{AEM}^{H}$ = 3 Ω·cm^2 , $\bar{R}_{CEM}^{D} = \bar{R}_{AEM}^{D}$= 26 Ω·$cm^2$) is short-circuited with an external load of 0.6 Ω. The initial concentrations of HS is 0.6 M and DS/LS is 0.02 M; the molar conductivity of HS is 0.009 m^2/Ω mol and DS/LS is 0.012 m^2/Ω·mol, while $\bar{V}_H$ is fixed at 1.

Fig. 5(a) presents the relationship between rejection and recovery for various membrane permselectivity, assuming the same membranes are used in RED and ED cells ($\alpha_{ED} = \alpha_{RED}$ = 0.3, 0.6, 0.9, or 1). For each given membrane permselectivity, there exists a clear tradeoff between the rejection and recovery of the overall REDD stack: greater rejection is generally obtained at the expense of lower recovery, and vice versa. Similar tradeoff relationships are also commonly observed in RO-based desalination plants, where higher recovery results in increased salinity of the brine and therefore lower apparent salt rejection [42]. Nevertheless, the tradeoff curves in traditional RO plants are much flatter since the apparent rejection is only mildly affected by the recovery. The much steep tradeoff lines for the REDD stack implies a narrower window for operation, which is a critical challenge to be further addressed.

We further investigated the case of allowing α_{ED} to be separately optimized while fixing α_{RED} at 0.9 (Fig. 5(b)). Decreasing α_{ED} from 1.0 to 0.3 results in a shift of the tradeoff line towards to upper right direction in Fig. 5(b), indicating a more favorable condition for desalination. However, further decrease in its value to 0.1 leads to a dramatic reduction in rejection/recovery performance. These results further confirm the findings from Fig. 4 that the use of moderately leaky ion exchange membranes in the ED_{cell} is beneficial in enhancing the desalination performance of REDD. Indeed, for α_{ED}

ranging from 0.3 to 0.6, rejections of close to 100 % can be achieved for recoveries up to 0.3, which greatly extends the desalination operating window of the REDD stack. The current work reveals the feasibility to produce fresh water with high quality at reasonable recovery by using well-designed membrane stack using IEMs with high permselectivity in the RED_{cell} and IEMs with moderate permselectivity (e.g., leaky IEMs) in the ED_{cell}. Even though the use of leaky IEMs in ED_{cell} has the tendency to slow down the process (Appendix A.2, Fig. A.2), this effect can be compensated by the low ionic resistance of leaky membranes (Appendix A.1, Fig. A.1 and A.2).

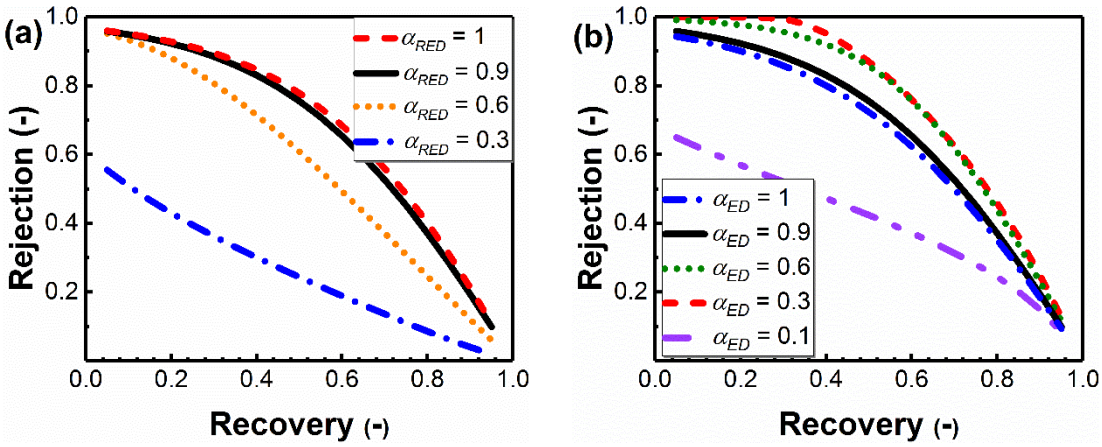

Fig. 5. Equivalent salt rejection (φ) (based on modelling work) of an REDD stack for varied fresh water recoveries (γ) ranging from 0 to 1: (a) φ versus γ for membranes in both RED_{cell} and ED_{cell} at a series of permselectivities (i.e., $\alpha_{RED} = \alpha_{ED}$) of 0.3, 0.6, 0.9, 1; (b) φ versus γ for membranes in the ED_{cell} at a series of permselectivities (α_{ED}) of 0.1, 0.3, 0.6, 0.9, 1, while fixing the membrane permselecitivity (α_{RED}) in the RED_{cell} at 0.9. The REDD stack (N = 5, A = 104 cm^2, $\lambda_H = \lambda_D$ = 0.2 mm, $\overline{R}_{CEM}^{H} = \overline{R}_{AEM}^{H}$ = 3 Ω·cm^2, $\overline{R}_{CEM}^{D} = \overline{R}_{AEM}^{D}$ = 26 Ω·cm^2) is short-circuited with an external load of 0.6 Ω. The initial concentrations of HS is 0.6 M and DS/LS is 0.02 M; the molar conductivity of HS is 0.009 m^2/Ω mol and DS/LS is 0.012 m^2/Ω·mol, while $\overline{V}_H$ is fixed at 1.

4.2 The effects of system operation conditions on desalination performance

We systematically investigated the effects of concentration ratios of HS over DS ($\bar{c}_{H0}$, up to 300) and volumetric ratios of HS over the sum of LS and DS ($\bar{V}_H$, ranging from 0.01 to 10) on desalination performance of REDD. For $\bar{V}_H \geqslant 0.1$, all cases show nearly identical rejection and recovery behavior (Fig. 6). Both parameters increase significantly as $\bar{c}_{H0}$ increases up to 60. With further increase in $\bar{c}_{H0}$, the rejection asymptotically approaches 1, which is accompanied with further enhanced recovery. This trend can be explained by greater electrical driving force at higher salinity gradient. Lower $\bar{V}_H$ (e.g., 0.01 and 0.03) can lead to dramatic reduction in rejection and recovery performance, which should be avoided.

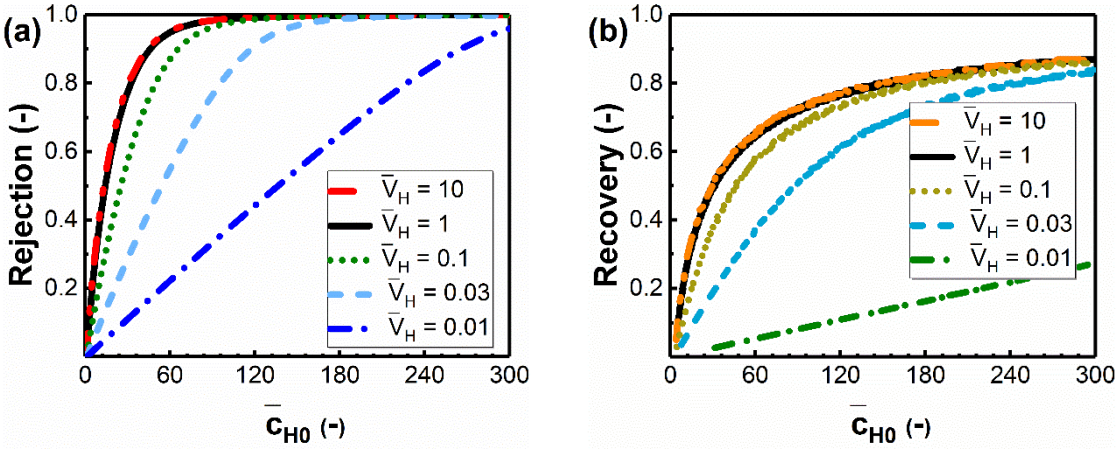

Fig. 6. Performance evaluation (based on modelling work) of an REDD stack with varied ratios of c_{HS} to c_{LS} ($\bar{C}_{H0}$), while the ratios of V_H to (V_L+V_D) ($\bar{V}_H$) are fixed at 10, 1, 0.1, 0.03 and 0.01: (a) equivalent salt rejection versus $\bar{C}_{H0}$ at a constant recovery of 0.67; (b) fresh water recovery versus $\bar{C}_{H0}$ at a constant rejection of around 0.95. The REDD stack (N = 5, A = 104 cm^2, λ_H = λ_D = 0.2 mm, $\bar{R}_{CEM}^{H}$ = $\bar{R}_{AEM}^{H}$ = 3 Ω·cm^2 , $\bar{R}_{CEM}^{D}$ = $\bar{R}_{AEM}^{D}$= 26 Ω·cm^2, α_{RED} = 0.9, α_{ED} = 0.3) is short-circuited with an external load of 0.6 Ω. The initial concentrations of DS/LS is 0.02 M; the molar conductivity of HS is 0.009 m^2/Ω mol and DS/LS is 0.012 m^2/Ω·mol.

Additional simulations on the effect of $\bar{V}_H$ at fixed $\bar{c}_{H0}$ values (10, 30 and 300) are summarized in Fig. 7. For each $\bar{c}_{H0}$, both rejection and recovery initially increase strongly with $\bar{V}_H$ and then reach a plateau. This increase can be attributed to the enhanced ability of the RED_{cell} to maintain a desirable electrical driving force for a longer time (Eq. (13)). The plateau of the recovery depends strongly on the concentration ratio. While a low maximum recovery of 0.2 is obtained at a concentration ratio of 10, the recovery can be as high as 0.9 at $\bar{c}_{H0}$ = 300. The trend to the plateau occurs at different volume ratios, with lower $\bar{V}_H$ required for higher $\bar{c}_{H0}$. For all case, the transition seems to occur at a $\bar{V}_H \cdot \bar{c}_{H0}$ value of approximately 10, which requires the initial ionic charge in the HS to be an order of magnitude higher than that in the LS and DS. The rejection behavior follows a similar trend.

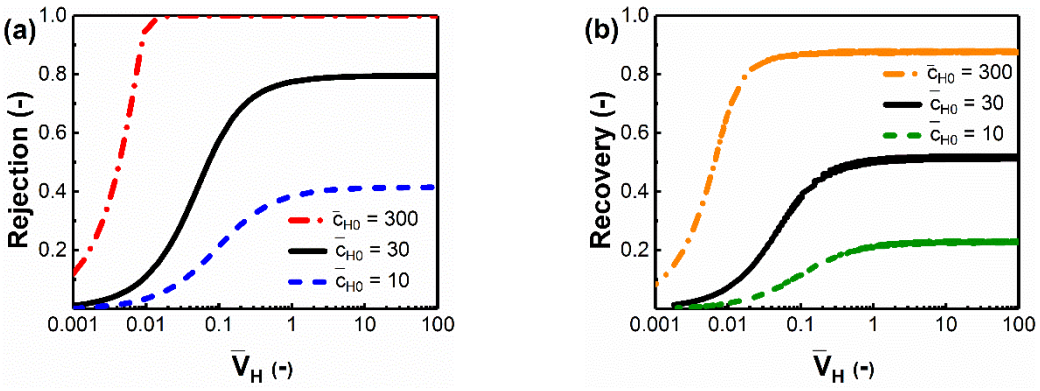

Fig. 7. Performance evaluation (based on modelling work) of an REDD stack with varied ratios of V_H to (V_L+V_D) ($\bar{V}_H$) while the ratios of c_{HS} to c_{LS} ($\bar{C}_{H0}$) are fixed at 300, 30, and 10: (a) equivalent salt rejection versus $\bar{V}_H$ at a constant recovery of 0.67; (b) fresh water recovery versus $\bar{V}_H$ at a constant rejection of around 0.95. The REDD stack (N = 5, A = 104 cm^2, λ_H = λ_D = 0.2 mm, $\bar{R}_{CEM}^{H}$ = $\bar{R}_{AEM}^{H}$ = 3 Ω·cm^2 , $\bar{R}_{CEM}^{D}$ = $\bar{R}_{AEM}^{D}$= 26 Ω·cm^2, α_{RED} = 0.9, α_{ED} = 0.3) is short-circuited with an external load of 0.6 Ω. The initial

concentrations of DS/LS is 0.02 M; the molar conductivity of HS is 0.009 m^2/Ω mol and DS/LS is 0.012 $m^2/\Omega \cdot mol$.

Fig. 8 presents a contour plot of desalination performance of the REDD stack as a function of $\bar{c}_{H0}$ and $\bar{V}_H$. Both peak rejection and recovery are attained at the upper right corner of the plot, indicating a better performance of the REDD stack by using greater driven force (i.e., greater $\bar{V}_H \cdot \bar{c}_{H0}$). Particularly, high rejection (e.g., $\varphi > 0.99$) can be obtained at the concentration ratio > 100 and $\bar{V}_H \cdot \bar{c}_{H0} > 10$. Based on these simulation results, a high concentration ratio ($\geqslant 30$) together with a moderate volume ratio ($\geqslant 0.5$) is recommended in order to achieve optimized rejection (e.g., $\varphi \geqslant 0.8$) and recovery (e.g., $\gamma \geqslant 0.5$) at the same time. These requirements are further confirmed by the rejection-recovery tradeoff lines in Fig. 9. Compared to the volume ratio, the concentration ratio plays a more significant role in extending the operational window for REDD. A high concentration ratio could potentially be met by co-locating the REDD process with seawater desalination facilities [6], where REDD treats the desalination brine to simultaneously mitigate the environmental impacts of brine discharge and provide driving force for REDD.

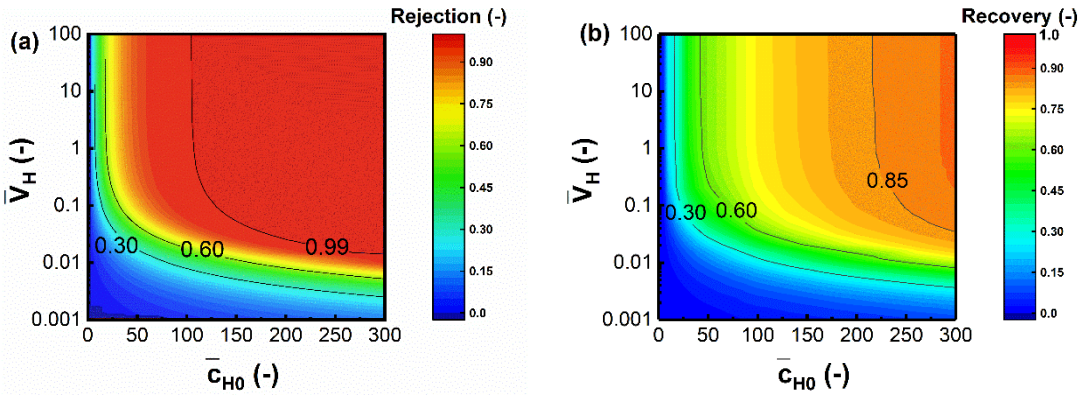

Fig. 8. Performance (based on modelling work) of an REDD stack as a function of varied ratios of c_{HS} to c_{LS} ($\bar{C}_{H0}$) and varied ratios of V_H to (V_L+V_D) ($\bar{V}_H$) (horizontal and vertical axes, respectively): (a) equivalent salt rejection versus $\bar{C}_{H0}$ and $\bar{V}_H$ at a constant recovery of 0.67; (b) fresh water recovery versus $\bar{C}_{H0}$ and $\bar{V}_H$ at a constant rejection of around 0.95. The REDD stack (N = 5, A = 104 cm^2, λ_H = λ_D = 0.2 mm, $\bar{R}_{CEM}^{H}$ = $\bar{R}_{AEM}^{H}$ = 3 Ω·cm^2 , $\bar{R}_{CEM}^{D}$ = $\bar{R}_{AEM}^{D}$= 26 Ω·cm^2, α_{RED} = 0.9, α_{ED} = 0.3) is short-circuited with an external load of 0.6 Ω. The initial concentrations of DS/LS is 0.02 M; the molar conductivity of HS is 0.009 m^2/Ω mol and DS/LS is 0.012 m^2/Ω·mol.

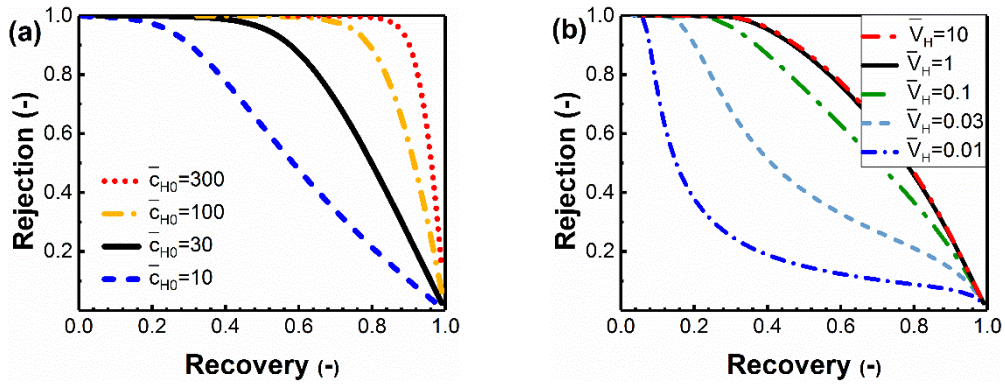

Fig. 9. Equivalent salt rejection (φ) (based on modelling work) of an REDD stack with varied fresh water recoveries (γ) ranging from 0 to 1: (a) φ versus γ for the ratios ($\bar{C}_{H0}$) of c_{HS} to c_{LS} at 300, 100, 30, and 10, while fixing $\bar{V}_H$ at 1; (b) φ versus γ while the ratios ($\bar{V}_H$) of V_{HS} to (V_L+V_D) are fixed at 10, 1, 0.1, 0.03 and 0.01. The REDD stack (N = 5, A = 104 cm^2, λ_H = λ_D = 0.2 mm, $\bar{R}_{CEM}^{H}$ = $\bar{R}_{AEM}^{H}$ = 3 Ω·cm^2 , $\bar{R}_{CEM}^{D}$ = $\bar{R}_{AEM}^{D}$= 26 Ω·cm^2, α_{RED} = 0.9, α_{ED} = 0.3) is short-circuited with an external load of 0.6 Ω. The initial concentrations of DS/LS is 0.02 M; the molar conductivity of HS is 0.009 m^2/Ω mol and DS/LS is 0.012 m^2/Ω·mol.

4.3 The effects of system configurations on desalination performance

Conventional desalination technology such as RO often uses a multi-stage configuration to enhance the water recovery. Similarly, a multi-pass configuration can be used to improve the overall salt rejection. In this section, we explore these strategies to further optimize the desalination performance of REDD (Fig. 10). In the multi-pass operation (Fig. 10(a)), the desalinated DS effluent (first pass) is applied as the influent

548 to a subsequent REDD process for further removal of salts (second pass). In this
549 configuration, the LS and HS can be refreshed in the later passes to maintain the
550 required driving force. As the salt concentration reduces after each additional pass, the
551 overall rejection improves but the overall recovery decreases (e.g., see the shift of
552 point A (1 pass) to point B (2 pass) in Fig. 11(a)). The corresponding tradeoff line
553 shifts slightly outwards as the number of passes increase, particularly over the recovery
554 range of 0.4 to 0.8. Considering a given overall recovery of 0.6, rejections of 0.88, 0.96,
555 and 0.99 can be obtained for 1-, 2-, and 3-pass treatment, respectively. Although the
556 multi-pass operation can slightly extend the operation window for desired
557 combinations of rejection and recovery, it involves substantially increased capital (e.g.,
558 increased membrane area) and operation cost (e.g., pumping). Therefore, its
559 application requires an acceptable balance between the technical benefits and cost
560 considerations.

561

562 In multi-stage operation, the LS effluent (equivalent to the concentrate in conventional
563 desalination) from an early stage is further treated in a next stage to recover additional
564 desalted water (Fig. 10(b)). As a result, this treatment can significantly increase the
565 overall recovery (e.g., see the shift of point C for a 1-stage treatment to point D for a 2-
566 stage treatment in Fig. 11(b)). In the current study, the use of a 3-stage treatment
567 allows a nearly complete salt rejection up to a recovery of 0.7, which is much wider
568 compared to the single-stage operation. It is important to note the sharp decline of
569 overall rejection at higher recovery (e.g., > 0.7 for the 3-stage configuration). In this
570 case, the use of an overly high recovery in an early stage produces a LS effluent
571 containing significant amount of salts, which results in dramatically reduced water
572 quality for the diluent water in the later stage(s) and therefore greatly reduced overall

573 rejection. To fully unleash the benefits of the multi-stage operation, the use of overall
574 high recovery in early stage(s) should be strictly avoided in practical desalination.

575

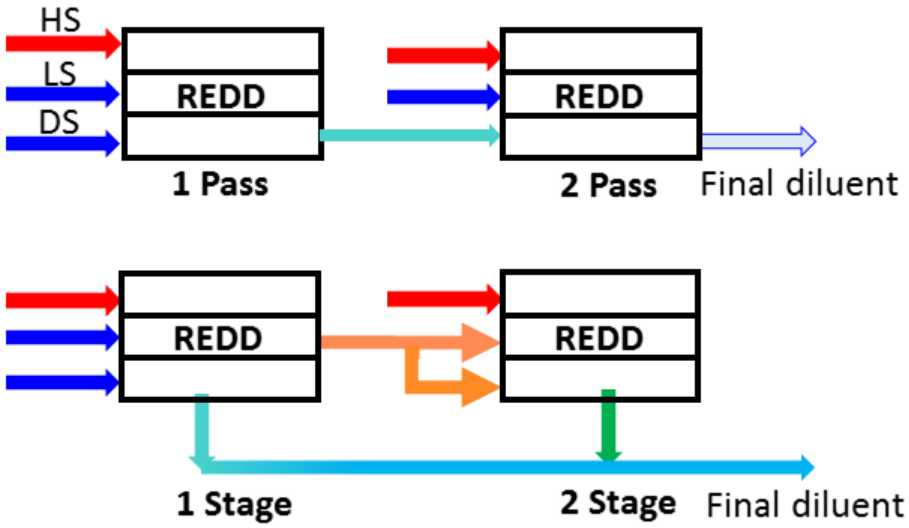

576

577 **Fig. 10. Schematic diagrams of the REDD systems with two basic configurations: (a) multi-pass mode in**
578 **which DS effluent of each pass was applied as the DS inffluent of the next pass, while LS and HS inffluent of**
579 **each pass were renewed simultaneously, leading to higher quality of final DS effluent; (b) multi-stage mode in**
580 **which LS effluent of each stage was redistributed to both DS and LS water channels of the next stage, while**
581 **HS inffluent of each stage are renewed simultaneously, leading to additional recovery of desalinated water.**

582

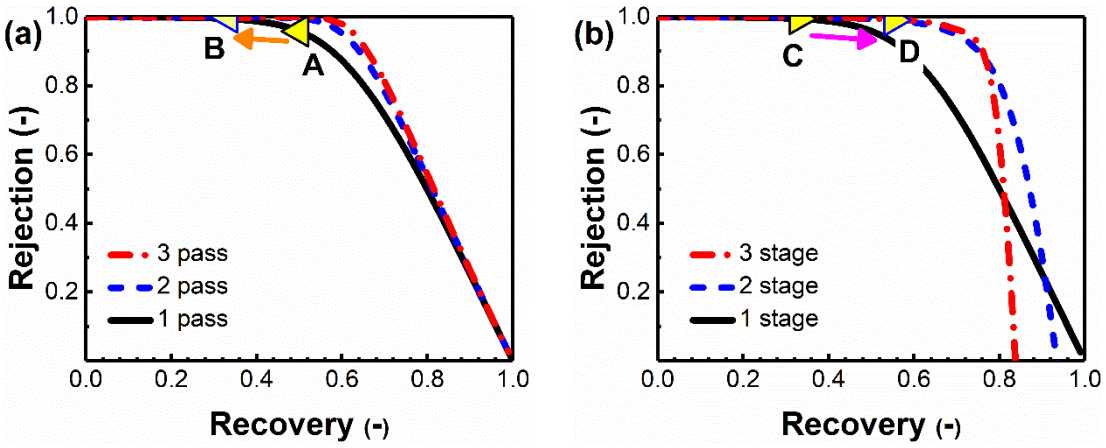

583

584 **Fig. 11. Equivalent salt rejection (φ) (based on modelling work) versus varied fresh water recoveries (γ)**

(ranging from 0 to 1) of an REDD system with multi-pass or multi-stage configurations: (a) φ versus γ in multi-pass operation, 1 pass, 2 pass, and 3 pass. At each pass, the initial concentrations of LS (C_{L0}) and DS (C_{D0}) are 0.02 M and the concentration of desalinated water in the last pass, respectively; (b) φ versus γ in multi-stage operation, 1 stage, 2 stage, and 3 stage. At each stage, both C_{L0} and C_{D0} equal to the concentration of treated LS in the last stage. The REDD stack (N = 5, A = 104 cm^2, $\lambda_H = \lambda_D$ = 0.2 mm, $\bar{R}_{CEM}^{H} = \bar{R}_{AEM}^{H}$ = 3 Ω·cm^2 , $\bar{R}_{CEM}^{D} = \bar{R}_{AEM}^{D}$= 26 Ω·cm^2, α_{RED} = 0.9, α_{ED} = 0.3) is short-circuited with an external load of 0.6 Ω. The initial concentrations of HS (C_{H0}) is the 30 times of C_{L0}; The molar conductivity of HS is 0.009 m^2/Ω mol and DS/LS is 0.012 m^2/Ω·mol, while $\bar{V}_H$ is fixed at 1.

5. Implications

In the recent literature, several other hybridization schemes involving desalination processes and SGE recovery technologies have been reported. One notable example is the RO-PRO hybrid[43, 44]. According to Yip et al. [26], PRO offers better energy efficiency compared to RED. Nevertheless, numerous studies have reported high fouling tendency [45-49] and mechanical instability of membranes [50-52] in PRO operation where low salinity waste water is convected to and through the membrane. In this respect, RED may provide more stable operation. A recent pilot RED plant in Italy did not observe any significant performance loss due to fouling and/or membrane decay [31]. Additional techniques such as charge reversal, widely used in the field of electrodialysis for fouling control by switching the ionic solute flow direction [53, 54], could also be explored to mitigate fouling if required [30, 55]. Furthermore, compared to the mechanical energy output from PRO that requires the use of pressure exchangers and hydroturbines in a relatively complex configuration, the direct electricity output from RED allows a simpler process scheme but also greater versatility in conditioning the output (e.g., serial vs. parellel connections, voltage amplifications, and DC to AC

conversion) [56]. Consequently, RED-based hybrid desalination schemes deserve further attention to fully unleash their potential.

Although the current study assumes the same membrane areas for the RED_{cell} and the ED_{cell}, this condition can be relaxed. For example, the use of greater number of membrane pairs in the RED_{cell} is expected to improve the equivalent salt rejection of the REDD stack thanks to the greater voltage output available to drive the ED process. In addition to the batch mode operation used in the current study, further investigations can be performed on the REDD process operating in a continuous mode. Additional studies are also required to explore the performance of REDD with various flow configurations (e.g., the choice of different feed streams, the implementation of partial recycling, etc.) to optimized system operation.

6. Conclusion

In this study, we report a novel self-sufficient desalination method based on the hybridization of RED and ED processes. A model was developed to simulate its desalination performance, which was verified by a series of bench-scale experiments. Our modeling work evaluates, for the first time, the rejection-recovery tradeoff for this novel RED-ED hybrid system. The simulation results demonstrate the general trend of decreased rejection at higher recovery. More favorable tradeoff curves can be obtained (1) by using tight IEMs in the RED_{cell} but relatively leaky IEMs in the ED_{cell} and (2) by applying greater driving force (e.g., using higher $\overline{c}_{H0}$ and $\overline{V}_H$), which significantly improves the operational window of the REDD. In addition, multi-pass and multi-stage schemes can be adopted to further enhance system rejection and recovery, respectively.

Our work highlights the technical feasibility as well as the practical constraints of the REDD technique, and provides important insights for the further development of this self-sufficient desalination technology.

Acknowledgements

The work described in this paper was substantially supported by a grant from the Research Grants Council of the Hong Kong Special Administration Region, China (C7051-17G). We also appreciate the Seed Funding for Strategic Interdisciplinary Research Scheme, the University of Hong Kong.

List of Symbols

N	number of the repeating unit in a REDD stack (N = 5 in the current study)
R	Gas constant (8.314 J/mol·K)
T	absolute temperature (K)
F	Fraday constant (96485 C/mol)
z_i	valence of specific ionic component i (-) ($z^+ = z^-$=1 for the model salt NaCl using in the current study)
c_{H0}	initial concentration of the high salinity stream (HS) (mol/L)
c_{Ht}	instant concentration of the high salinity stream (HS) (mol/L)
c_{Hf}	final concentration of the high salinity stream (HS) (mol/L)
c_{L0}	initial concentration of the low salinity stream (LS) (mol/L)
c_{Lt}	instant concentration of the low salinity stream (LS) (mol/L)
c_{Lf}	final concentration of the low salinity stream (LS) (mol/L)
c_{D0}	initial concentration of the diluent stream (LS) (mol/L)
c_{Dt}	instant concentration of the diluent stream (LS) (mol/L)
c_{Df}	final concentration of the diluent stream (LS) (mol/L)
f	equilibrium constant of the concentration ratio of finalized HS to LS (-)

J current density in the REDD stack (A/m^2)

E_{net} electromotive force generated by the REDD stack (V)

A cross-sectional area of the ion exchange membranes in the stack ($0.0104 m^2$)

R_{stack} electrical resistance of the REDD stack (Ω)

$R_{external}$ electrical resistance of the external load in the electrical circuit (Ω)

$\overline{R}_{RED}^{CEM}$ area resistance of the cation exchange membranes in the RED_{cell} ($\Omega \cdot m^2$)

$\overline{R}_{RED}^{AEM}$ area resistance of the anion exchange membrane in the RED_{cell} ($\Omega \cdot m^2$)

$\overline{R}_{ED}^{CEM}$ area resistance of the cation exchange membranes in the ED_{cell} ($\Omega \cdot m^2$)

$\overline{R}_{ED}^{AEM}$ area resistance of the anion exchange membrane in the ED_{cell} ($\Omega \cdot m^2$)

T_{co}^{s} transport number of the co-ions of a certain ion exchange membrane in the bulk solution (-)

T_{co}^{m} transport number of the co-ions of a certain ion exchange membrane in the membrane matrix (-)

T_{ct}^{s} transport number of the counter-ions of a certain ion exchange membrane in the bulk solution (-)

T_{ct}^{m} transport number of the counter-ions of a certain ion exchange membrane in the membrane matrix (-)

j_{co} ionic flux of the co-ions of a certain ion exchange membrane ($mol/m^2 s$)

j_{ct} ionic flux of the counter-ions of a certain ion exchange membrane ($mol/m^2 s$)

j_{mass}^{H} mass flux of the high salinity stream ($mol/m^2 s$)

j_{mass}^{L} mass flux of the low salinity stream ($mol/m^2 s$)

j_{mass}^{L} mass flux of the diluent stream ($mol/m^2 s$)

V_H volume of the high salinity stream (L)

V_L volume of the low salinity stream (mol/L)

V_D volume of the diluent stream (mol/L)

$\bar{q}$ salt removal efficiency of the REDD stack (-)

$\bar{c}_{H0}$ salinity ratio of c_{H0} to c_{D0} (-)

$\bar{V}_H$ volumetric ratio of V_H to $(V_L + V_D)$ (-)

V_A^D ratio of DS volume to total membrane area (L/cm^2)

Greek letters

α_{RED}^{CEM} permselectivity of the cation exchange membranes in the RED$_{cell}$ (-)

α_{RED}^{AEM} permselectivity of the anion exchange membranes in the RED$_{cell}$ (-)

α_{RED} averaged membrane permselectivity in the RED$_{cell}$ (-)

α_{ED}^{CEM} permselectivity of the cation exchange membranes in the ED$_{cell}$ (-)

α_{ED}^{AEM} permselectivity of the anion exchange membranes in the ED$_{cell}$ (-)

α_{ED} averaged membrane permselectivity in the ED$_{cell}$ (-)

λ_H inter-membrane distance of the high salinity stream in the REDD stack (m)

λ_L inter-membrane distance of the low salinity stream in the REDD stack (m)

λ_D inter-membrane distance of the diluent stream in the REDD stack (m)

σ_H molar conductivity of the high salinity stream (m^2/Ω·mol)

σ_L molar conductivity of the low salinity stream (m^2/Ω·mol)

σ_D molar conductivity of the diluent stream (m^2/Ω·mol)

γ fresh water recovery of the REDD stack (-)

φ equivalent salt rejection of the REDD stack (-)

References

[1] M. Elimelech, W.A. Phillip, The future of seawater desalination: energy, technology, and the environment, Science, 333 (2011) 712-717.

[2] W. Li, W.B. Krantz, E.R. Cornelissen, J.W. Post, A.R.D. Verliefde, C.Y. Tang, A novel hybrid process of reverse electrodialysis and reverse osmosis for low energy seawater desalination and brine management, Appl. Energy, 104 (2013) 592-602.

[3] B.E. Logan, The Global Challenge of Sustainable Seawater Desalination, Environ. Sci. Technol. Lett., (2017).

[4] M. Tedesco, E. Brauns, A. Cipollina, G. Micale, P. Modica, G. Russo, J. Helsen, Reverse electrodialysis with saline waters and concentrated brines: A laboratory investigation towards technology scale-up, J. Membr. Sci., 492 (2015) 9-20.

[5] Q. Chen, Y.-Y. Liu, C. Xue, Y.-L. Yang, W.-M. Zhang, Energy self-sufficient desalination stack as a potential fresh water supply on small islands, Desalination, 359 (2015) 52-58.

[6] Y. Mei, C.Y. Tang, Co-locating reverse electrodialysis with reverse osmosis desalination: Synergies and implications, J. Membr. Sci., 539 (2017) 305-312.

[7] Ramato A. Tufa, E. Curcio, E. Brauns, W. van Baak, E. Fontananova, G. Di Profio, Membrane Distillation and Reverse Electrodialysis for Near-Zero Liquid Discharge and low energy seawater desalination, J. Membr. Sci., 496 (2015) 325-333.

[8] B.E. Logan, M. Elimelech, Membrane-based processes for sustainable power generation using water, Nature, 488 (2012) 313-319.

[9] F. Luo, Y. Wang, C. Jiang, B. Wu, H. Feng, T. Xu, A power free electrodialysis (PFED) for desalination, Desalination, 404 (2017) 138-146.

[10] M. Ye, M. Pasta, X. Xie, K.L. Dubrawski, J. Xu, C. Liu, Y. Cui, C.S. Criddle, Charge-Free Mixing Entropy Battery Enabled by Low-Cost Electrode Materials, ACS Omega, 4 (2019) 11785-11790.

[11] J.W. Post, J. Veerman, H.V.M. Hamelers, G.J.W. Euverink, S.J. Metz, K. Nymeijer, C.J.N. Buisman, Salinity-gradient power: Evaluation of pressure-retarded osmosis and reverse electrodialysis, J. Membr. Sci., 288 (2007) 218-230.

[12] G.Z. Ramon, B.J. Feinberg, E.M.V. Hoek, Membrane-based production of salinity-gradient power, Energy Environ. Sci., 4 (2011) 4423.

[13] R.A. Tufa, S. Pawlowski, J. Veerman, K. Bouzek, E. Fontananova, G. di Profio, S. Velizarov, J. Goulão Crespo, K. Nijmeijer, E. Curcio, Progress and prospects in reverse electrodialysis for salinity gradient energy conversion and storage, Appl. Energy, 225 (2018) 290-331.

[14] Y. Mei, C.Y. Tang, Recent developments and future perspectives of reverse electrodialysis technology: A review, Desalination, 425 (2018) 156-174.

[15] Q. Wang, X. Gao, Y. Zhang, Z. He, Z. Ji, X. Wang, C. Gao, Hybrid RED/ED system: Simultaneous osmotic energy recovery and desalination of high-salinity wastewater, Desalination, 405 (2017) 59-67.

[16] Y. Kim, B.E. Logan, Hydrogen production from inexhaustible supplies of fresh and salt water using microbial reverse-electrodialysis electrolysis cells, Proceedings of the National Academy of Sciences of the United States of America, 108 (2011) 16176-16181.

[17] J.Y. Nam, R.D. Cusick, Y. Kim, B.E. Logan, Hydrogen generation in microbial reverse-electrodialysis electrolysis cells using a heat-regenerated salt solution, Environ. Sci. Technol., 46 (2012) 5240-5246.

[18] X. Zhu, M.C. Hatzell, R.D. Cusick, B.E. Logan, Microbial reverse-

754 electrodialysis chemical-production cell for acid and alkali production, Electrochem.
755 Commun., 31 (2013) 52-55.
756 [19] X. Luo, F. Zhang, J. Liu, X. Zhang, X. Huang, B.E. Logan, Methane production
757 in microbial reverse-electrodialysis methanogenesis cells (MRMCs) using thermolytic
758 solutions, Environ. Sci. Technol., 48 (2014) 8911-8918.
759 [20] X. Li, I. Angelidaki, Y. Zhang, Salinity-gradient energy driven microbial
760 electrosynthesis of value-added chemicals from CO2 reduction, Water Res, 142 (2018)
761 396-404.
762 [21] R. Long, B. Li, Z. Liu, W. Liu, Hybrid membrane distillation-reverse
763 electrodialysis electricity generation system to harvest low-grade thermal energy, J.
764 Membr. Sci., 525 (2017) 107-115.
765 [22] A. Ali, R.A. Tufa, F. Macedonio, E. Curcio, E. Drioli, Membrane technology in
766 renewable-energy-driven desalination, Renew. Sust. Energ. Rev., 81 (2018) 1-21.
767 [23] J. Hu, S. Xu, X. Wu, D. Wu, D. Jin, P. Wang, Q. Leng, Theoretical simulation
768 and evaluation for the performance of the hybrid multi-effect distillation—reverse
769 electrodialysis power generation system, Desalination, 443 (2018) 172-183.
770 [24] M. Chen, Y. Mei, Y. Yu, R.J. Zeng, F. Zhang, S. Zhou, C.Y. Tang, An internal-
771 integrated RED/ED system for energy-saving seawater desalination: A model study,
772 Energy, 170 (2019) 139-148.
773 [25] Q. She, X. Jin, C.Y. Tang, Osmotic power production from salinity gradient
774 resource by pressure retarded osmosis: Effects of operating conditions and reverse
775 solute diffusion, J. Membr. Sci., 401-402 (2012) 262-273.
776 [26] N.Y. Yip, M. Elimelech, Comparison of energy efficiency and power density in
777 pressure retarded osmosis and reverse electrodialysis, Environ Sci Technol, 48 (2014)
778 11002-11012.
779 [27] N.Y. Yip, D. Brogioli, H.V. Hamelers, K. Nijmeijer, Salinity Gradients for
780 Sustainable Energy: Primer, Progress, and Prospects, Environ. Sci. Technol., 50 (2016)
781 12072-12094.
782 [28] Q. She, R. Wang, A.G. Fane, C.Y. Tang, Membrane fouling in osmotically
783 driven membrane processes: A review, J. Membr. Sci., 499 (2016) 201-233.
784 [29] M. Zhang, D. Hou, Q. She, C.Y. Tang, Gypsum scaling in pressure retarded
785 osmosis: experiments, mechanisms and implications, Water Res, 48 (2014) 387-395.
786 [30] D.A. Vermaas, D. Kunteng, M. Saakes, K. Nijmeijer, Fouling in reverse
787 electrodialysis under natural conditions, Water Res, 47 (2013) 1289-1298.
788 [31] M. Tedesco, C. Scalici, D. Vaccari, A. Cipollina, A. Tamburini, G. Micale,
789 Performance of the first reverse electrodialysis pilot plant for power production from
790 saline waters and concentrated brines, J. Membr. Sci., 500 (2016) 33-45.
791 [32] L. Cao, W. Guo, W. Ma, L. Wang, F. Xia, S. Wang, Y. Wang, L. Jiang, D. Zhu,
792 Towards understanding the nanofluidic reverse electrodialysis system: well matched
793 charge selectivity and ionic composition, Energy Environ. Sci., 4 (2011) 2259.
794 [33] J. Veerman, R.M. de Jong, M. Saakes, S.J. Metz, G.J. Harmsen, Reverse
795 electrodialysis: Comparison of six commercial membrane pairs on the thermodynamic
796 efficiency and power density, J. Membr. Sci., 343 (2009) 7-15.
797 [34] P. Dlugolecki, K. Nymeijer, S. Metz, M. Wessling, Current status of ion
798 exchange membranes for power generation from salinity gradients, J. Membr. Sci.,
799 319 (2008) 214-222.
800 [35] N.Y. Yip, D.A. Vermaas, K. Nijmeijer, M. Elimelech, Thermodynamic, energy
801 efficiency, and power density analysis of reverse electrodialysis power generation
802 with natural salinity gradients, Environ. Sci. Technol., 48 (2014) 4925-4936.
803 [36] J. Veerman, M. Saakes, S.J. Metz, G.J. Harmsen, Electrical power from sea and

river water by reverse electrodialysis: a first step from the laboratory to a real power plant, Environ. Sci. Technol., 44 (2010) 9207-9212.
[37] H. Strathmann, Electrochemical and thermodynamic fundamentals, in: H. Strathmann (Ed.) Ion-exchange membrane separation processes, Elsevier B.V., Hungary, 2004.
[38] M. Tedesco, H.V.M. Hamelers, P.M. Biesheuvel, Nernst-Planck transport theory for (reverse) electrodialysis: I. Effect of co-ion transport through the membranes, J. Membr. Sci., 510 (2016) 370-381.
[39] E. Güler, R. Elizen, D.A. Vermaas, M. Saakes, K. Nijmeijer, Performance-determining membrane properties in reverse electrodialysis, J. Membr. Sci., 446 (2013) 266-276.
[40] E. Guler, Y. Zhang, M. Saakes, K. Nijmeijer, Tailor-made anion-exchange membranes for salinity gradient power generation using reverse electrodialysis, ChemSusChem, 5 (2012) 2262-2270.
[41] J. Gi Hong, S. Glabman, Y. Chen, Effect of inorganic filler size on electrochemical performance of nanocomposite cation exchange membranes for salinity gradient power generation, J. Membr. Sci., 482 (2015) 33-41.
[42] A.G. Fane, C.Y. Tang, R. Wang, Membrane Technology for Water: Microfiltration, Ultrafiltration, Nanofiltration, and Reverse Osmosis, in: Treatise on Water Science, 2010, pp. 301-335.
[43] V.S. Sim, Q. She, T.H. Chong, C.Y. Tang, A.G. Fane, W.B. Krantz, Strategic Co-Location in a Hybrid Process Involving Desalination and Pressure Retarded Osmosis (PRO), Membranes, 3 (2013) 98-125.
[44] J. Kim, M. Park, S.A. Snyder, J.H. Kim, Reverse osmosis (RO) and pressure retarded osmosis (PRO) hybrid processes: Model-based scenario study, Desalination, 322 (2013) 121-130.
[45] D.I. Kim, J. Kim, H.K. Shon, S. Hong, Pressure retarded osmosis (PRO) for integrating seawater desalination and wastewater reclamation: Energy consumption and fouling, J. Membr. Sci., 483 (2015) 34-41.
[46] G. Han, J. Zhou, C. Wan, T. Yang, T.S. Chung, Investigations of inorganic and organic fouling behaviors, antifouling and cleaning strategies for pressure retarded osmosis (PRO) membrane using seawater desalination brine and wastewater, Water Res, 103 (2016) 264-275.
[47] Q. She, Y.K.W. Wong, S. Zhao, C.Y. Tang, Organic fouling in pressure retarded osmosis: Experiments, mechanisms and implications, J. Membr. Sci., 428 (2013) 181-189.
[48] S.C. Chen, C.F. Wan, T.-S. Chung, Enhanced fouling by inorganic and organic foulants on pressure retarded osmosis (PRO) hollow fiber membranes under high pressures, J. Membr. Sci., 479 (2015) 190-203.
[49] N.Y. Yip, M. Elimelech, Influence of natural organic matter fouling and osmotic backwash on pressure retarded osmosis energy production from natural salinity gradients, Environ Sci Technol, 47 (2013) 12607-12616.
[50] Q. She, D. Hou, J. Liu, K.H. Tan, C.Y. Tang, Effect of feed spacer induced membrane deformation on the performance of pressure retarded osmosis (PRO): Implications for PRO process operation, J. Membr. Sci., 445 (2013) 170-182.
[51] Q. She, J. Wei, N. Ma, V. Sim, A.G. Fane, R. Wang, C.Y. Tang, Fabrication and characterization of fabric-reinforced pressure retarded osmosis membranes for osmotic power harvesting, J. Membr. Sci., 504 (2016) 75-88.
[52] Y. Li, R. Wang, S. Qi, C. Tang, Structural stability and mass transfer properties of pressure retarded osmosis (PRO) membrane under high operating pressures, J.

Membr. Sci., 488 (2015) 143-153.
[53] R.P. Allison, Electrodialysis reversal in water reuse applications, Desalination, 103 (1995) 11-18.
[54] S. Suwal, J. Amiot, L. Beaulieu, L. Bazinet, Effect of pulsed electric field and polarity reversal on peptide/amino acid migration, selectivity and fouling mitigation, Journal of Membrane Science, 510 (2016) 405-416.
[55] D.A. Vermaas, D. Kunteng, J. Veerman, M. Saakes, K. Nijmeijer, Periodic feedwater reversal and air sparging as antifouling strategies in reverse electrodialysis, Environ Sci Technol, 48 (2014) 3065-3073.
[56] Y. Huang, Y. Mei, S. Xiong, S.C. Tan, C.Y.Y. Tang, S.Y. Hui, Reverse Electrodialysis Energy Harvesting System Using High-Gain Step-Up DC/DC Converter, IEEE Trans. Sustain. Energy, 9 (2018) 1578-1587.

Appendix A

A.1. Ion exchange membranes (IEMs) and their critical properties reported in the context of reverse electrodialysis (RED).

Table A.1. presents the key parameters of both the commercial and tailor-made ion exchange membranes which have been investigated and tested in the RED stack.

Table A.1. A summary of state-of-art ion exchange membranes including commercial and tailor-made membranes reported in the literature.

Membrane pairs	Resistance[a]	Permselectivity[b]	References
CMH-PES/AMH-PES	9.50	0.92	[1-4]
QIANQIU CEM/AEM	2.41	0.84	[5]
CMV/AMV	2.72	0.93	[6, 7]
FKD/FAD	1.52	0.88	[1, 4, 7]
FKS/FAS	1.27	0.92	[8, 9]
CMX/AMX	2.63	0.95	[7, 10, 11]
CM-1/AM-1	2.29	0.98	[12]
CMI 7001/AMI 7001	3.47	0.92	[13]
V1 CEM/V1 AEM	1.60	0.93	[14]
DF-120 CEMs/DF-120 AEMs	1.70	0.95	[15]
PC-SK/PC-SA	2.15	0.94	[16]
CEM-80050-05/AEM-80045-01	2.19	0.96	[16-19]
CSO/ASV	2.98	0.95	[20, 21]
CMX/aPPO-20	6.24	0.94	[22]
CMX/aPPO-24	4.10	0.95	[22]
CMX/aPPO-27	4.40	0.94	[22]
CMX/aPPO-C6D2	16.08	0.95	[22]
CMX/aPPO-C6D6	3.05	0.92	[22]
CMX/aRadel-1.76	5.75	0.94	[22]
CMX/aRadel-1.87	4.38	0.93	[22]
CMX/aRadel-2.66	2.26	0.92	[22]

CMX/PECH B-2	1.93	0.93	[23]
CMX/PECH B-3	2.12	0.93	[23]
CMX/PECH B-1	1.87	0.93	[23]
CMX/PECH C	2.03	0.89	[23]
CMX/PECH A	2.48	0.95	[23]
A-sPPO/AMX	2.30	0.93	[10]
D-sPPO/AMX	2.57	0.94	[10]
P-sPPO/AMX	3.05	0.93	[10]

[a] Membrane resistance is measured in an electrolyte solution of 0.5 M NaCl at 25℃.

[b] Membrane permselectivity is measured over an concentration difference of 0.5 M and 0.1 M NaCl at 25℃.

Fig. A.1 shows the membrane permselectivity and ionic conductivity (i.e., 1/R) of the IEMs reported in previous literature on RED. There is an obvious tradeoff between membrane permselectivities and their resistance for both commercial and tailored ion exchange membranes. Specifically, ion exchange membrane with high permselectivity generally tends to have low ionic conductivity, and vice versa.

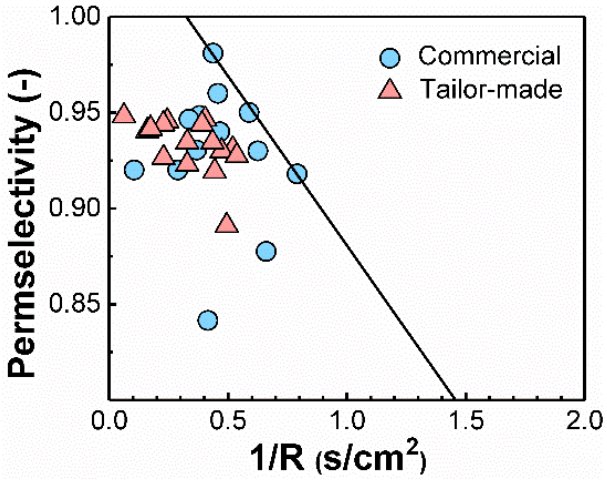

Fig. A.1 The membrane permselectivity and ionic conductivity of ion exchange membranes reported in previous literature on reverse electrodialysis.

A.2.The effects of membrane resistance on desalination performance of the energy self-sufficient RED-ED desalination (REDD) stack.

The membrane area (A) and/or time (T) required for achieving an equilibrium state was represented by the value of $A{\cdot}T$ product. The dependency of $A{\cdot}T$ product on membrane resistance was simulated with increasing membrane permselectivity (α_{ED}) in the ED_{cell} from 0.1 to 0.9 and fixing membrane permselectivity in the RED_{cell} at 0.9. Fig. A.2 demonstrates that $A{\cdot}T$ product can be reduced by decreasing membrane resistance for a specific α_{ED}. While the deterioration of membrane permselectivity in ED_{cell} has an adverse effect on the $A{\cdot}T$ product.

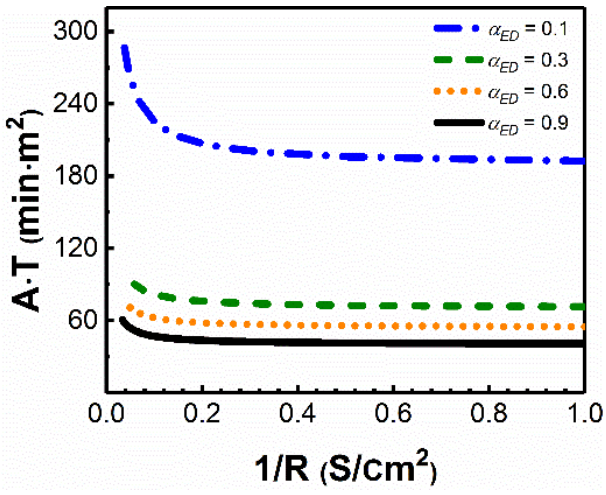

Fig. A.2. The product of membrane area and time (i.e., A·T) required for achieving an equilibrium state versus membrane resistance, while membrane permselectivity (α_{ED}) in the ED_{cell} at 0.1, 0.3, 0.6, 0.9 and membrane permselecitivity (α_{RED}) in the RED_{cell} at a constant value of 0.9. The REDD stack (N = 5, A = 104 cm², $\lambda_H = \lambda_D$ = 0.2 mm, $\bar{R}_{CEM}^{H} = \bar{R}_{AEM}^{H}$ = 3 Ω·cm² , $\bar{R}_{CEM}^{D} = \bar{R}_{AEM}^{D}$= 26 Ω·cm²) is short-circuited with an external load of 0.6 Ω. The initial concentrations of HS is 0.6 M and DS/LS is 0.02 M; the molar conductivity of HS is 0.009 m²/Ω mol and DS/LS is 0.012 m²/Ω·mol, while the recovery and $\bar{V}_H$ are fixed at 1/3 and 1, respectively.

A.3. The typical discharge curves of the REDD systems with multi-pass and multi-stage configurations.

The multi-pass and multi-stage configurations are investigated in the context of RED for the enhancement on the overall desalination performance. The representative discharge curves of these two system configurations are presented in Fig. A.3 and Fig. A.4, respectively, based on the operation scenario of using seawater (0.6 M NaCl) as HS and river water or brackish (0.02 M NaCl) as LS/DS.

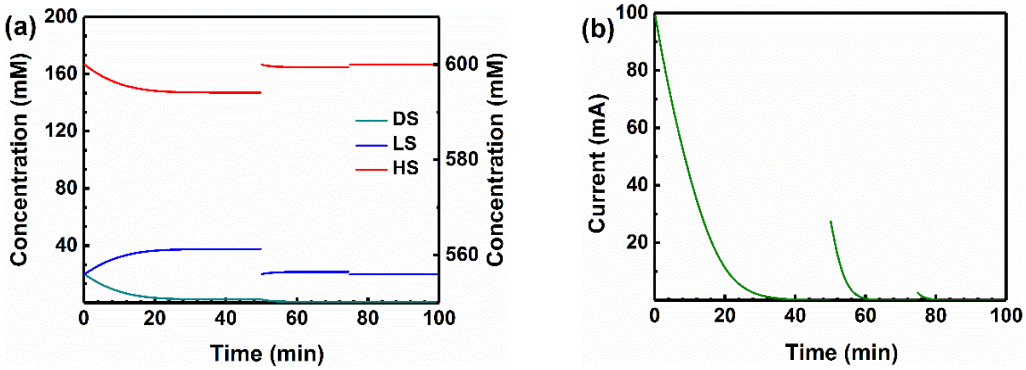

Fig. A.3. Typical discharge curves of an REDD system with 3-pass configuration: DS effluent of each pass was supplied as DS influent of the next pass, while renewing LS and HS simultaneously. The REDD stack at each pass (N = 5, A = 104 cm^2, $\lambda_H = \lambda_D$ = 0.2 mm, $\bar{R}_{CEM}^{H} = \bar{R}_{AEM}^{H}$ = 3 Ω·cm^2, $\bar{R}_{CEM}^{D} = \bar{R}_{AEM}^{D}$= 26 Ω·cm^2, $\alpha_{RED} = \alpha_{ED}$ = 0.9) is short-circuited with an external load of 0.6 Ω. The initial concentrations of HS and LS are 0.6 M and 0.02 M, respectively; the desalinated DS in each pass is further treated in the subsequent step for higher water quality; the molar conductivity of HS is 0.009 m^2/Ω mol and DS/LS is 0.012 m^2/Ω·mol, while the recovery and $\bar{V}_H$ are fixed at 1/3 and 1, respectively.

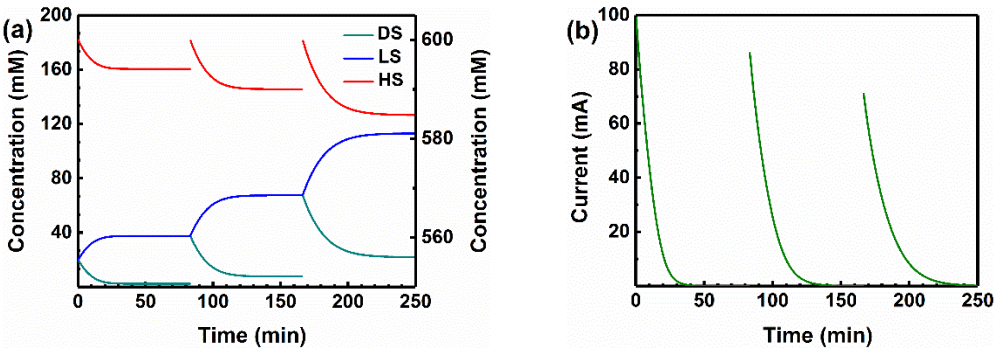

926

927 **Fig. A.4. Typical discharge curves of an REDD system with 3-stage configuration: LS effluent at each stage**
928 **was redistributed to the influent of both DS and LS in the following stage, while refreshing HS**
929 **simultaneously. The REDD stack at each stage (*N* = 5, *A* = 104 cm^2, $\lambda_H = \lambda_D$ = 0.2 mm, $\overline{R}_{CEM}^{H} = \overline{R}_{AEM}^{H}$ = 3**
930 **Ω·cm^2 , $\overline{R}_{CEM}^{D} = \overline{R}_{AEM}^{D}$= 26 Ω·cm^2, α_{RED} = 0.9, α_{ED} = 0.3) is short-circuited with an external load of 0.6 Ω.**
931 **The initial concentration of HS is 0.6 M; the LS effluent in each stage is used as influent of DS and LS in the**
932 **subsequent step for more desalinated water; the molar conductivity of HS is 0.009 m^2/Ω mol and DS/LS is**
933 **0.012 m^2/Ω·mol, while the recovery and $\overline{V}_H$ are fixed at 1/3 and 1, respectively.**

934